

RF-PLASMA PROTECTIVE COATING ON SILVER- COPPER ALLOYS USING HDMSO/O₂/AR PRECURSORS

Abd EL-Moaz, Y.^{1(*)}, Mohamed, W.¹, Rifai, M.¹, Morgan, N.^{2,3} & Abdel Ghany, N.⁴

¹Conservation dept., Faculty of Archaeology, Cairo Univ., Giza, Egypt

²Plasma Center, Al-Azhar Univ., Cairo, Egypt.

³Physics dept., Faculty of Science, Al-Azhar Univ., Cairo, Egypt.

⁴Physical Chemistry dept., National Research Centre, Dokki, Cairo, Egypt

E-mail address: yasmin97@cu.edu.eg

Article info.

Article history:

Received: 21-9-2022

Accepted: 16-12-2022

Doi: 10.21608/ejars.2023.305187

Keywords:

Plasma enhanced chemical vapor deposition(PECVD)

Thin Films

Adhesion

Silicon dioxide

Argon

Ellipsometry

EJARS – Vol. 13 (1) – June 2023: 61-74

Abstract:

Due to its excellent adherence to the metal substrate, Hexamethyldisiloxan was employed in the present study to create transparent barrier coating films that protect metal artifacts from corrosion. The deposition procedure used radio frequency plasma enhanced chemical vapor deposition (RF-PECVD). Using scanning electron microscopy combined with energy dispersive X-ray (SEM-EDX) and Fourier-transform infrared spectroscopy (FT-IR), the surfaces of the deposited films were identified and characterized. Atomic force microscopy was used to examine surface topography and roughness (AFM). Water contact angle measurement was used to determine the hydrophobic property (WCA). Moreover, a spectroscopic ellipsometer was used to measure the film's thickness (SE). Following the Siloxane protective layer's PECVD deposition, colorimetric measurement (CM) was utilized to assess surface appearance alterations. Electr-ochemical impedance spectroscopy (EIS) was used to study how siloxane coatings for metal substrates protect against corrosion as a function of RF power and gas input composition. It was found that the siloxane thin film's adhesion characteristics to the silver-copper alloy substrate were affected by the substrate pretreatment process and the consumed power during the deposition process.

1. Introduction

Silver and its alloys are regarded as ideal ductile materials widely used in the production of various precious and decorative artifacts, such as jewelry, coins, and silver tableware [1,2]. Organic coatings are frequently used to create a physical barrier between the metallic substrate and corrosive environments [3]. However, they are permeable to corrosive substances, such as Cl⁻, O₂, and H₂O, as water molecules at the coating–substrate interface may cause electrochemical

corrosion of metal beneath the coating, resulting in decreased adhesion strength and coating delamination [4]. As a result, the barrier properties of a coating are determined by three factors:

- 1) The coatings water sorption
- 2) Water transport within the coating
- 3) Water ease of access to the coating–substrate interface [5].

Thus, a well-known and low temperature technique for depositing SiO₂ and Si_xO_yC_z thin

films is plasma-enhanced chemical vapor deposition (PECVD) for applications requiring a low substrate temperature, such as the production of water-repellent silicon films coatings for the abrasion protection of various substrates [6]. Silicon dioxide (SiO_2) or silicon oxide (SiO) coatings are well-known for their resistance to gas and water vapor permeation. As an organosilicon reagent for PECVD of silicon compound thin films, hexamethyldisiloxane (HMDSO), a linear polydisiloxane, was proposed [7]. It has grown in popularity over the last decade due to its lower cost and higher deposition rates compared to similar silicon containing monomers [8]. Compared to silane compounds, HMDSO ($\text{C}_6\text{H}_{18}\text{OSi}_2$) is a simple and safe monomer to work with [9,10]. Plasma processes may be a promising clean technology for metal protection and may be proposed as a replacement for conventional methods, which are sometimes associated with serious environmental concerns [11]. The RF (13.56 MHz) plasmas own reasonably high plasma density at low temperature, which can facilitate the gas-phase formation of particulate matters requisite for depositing corrosion resistance films with structured rough surfaces while retaining functional hydrophobic surface groups, like C_xH_y or CF_x [12]. The polymerization of HMDSO caused by plasma treatment results in the formation of nanoparticles that are waterproof and have large static water contact angles [13]. Additionally, depending on the deposition conditions and progressive admixture of reactive gases, such as oxygen, the resulting film properties range from hydrophobic, poly (dimethylsiloxane)-like (PDMS-like), to more hydrophilic and nanoporous, and finally to more inorganic hard films based on a stable SiOSi backbone with only a limited amount of residual hydrocarbon groups [14]. The plasma chemistry leading from HMDSO/ O_2 or HMDSO/Ar gas mixtures to SiO_2 films has not been very well understood yet. Therefore,

the present paper aims to perform a comparative study of the growth process of protective thin films from HMDSO/ O_2 between the pre-activated and deposited silver-copper alloy substrate using argon plasma and the pre-activated silver-copper alloy substrate with argon and deposited with a mixture of oxygen and HMDSO at different power and time. Besides, it investigates pre-treatment using argon plasma, which removes organic contaminations from the surface, provides a buffer layer by creating active catalytic points, and improves the coating-substrate adhesion by physical sputtering. The coating films are also investigated using the EIS technique to evaluate the corrosion protection of the metal provided by the deposited films. To improve the quality of the deposited layers, PECVD processes can be optimized by varying some deposition (i.e., temperature, total and partial pressures, plasma power and frequency, etc.) and post-deposition (temperature and environment of the annealing process) parameters [15-17]. In this work, we present some results on the chemical and structural properties of SiO_2 thin films prepared by PECVD from HMDSO precursors. We mainly conducted a comparative study of the growth process of the protective thin films from HMDSO/ O_2 between the pre-activated and deposited silver-copper alloy substrate using argon plasma and the pre-activated silver-copper alloy substrate with argon and deposited with a mixture of oxygen and HMDSO at different power and time. Besides, the paper investigates pre-treatment using argon plasma, which removes organic contaminations from the surface, provides a buffer layer by creating active catalytic points, and improves the coating-substrate adhesion by physical sputtering. The coating films are also investigated using the EIS technique to evaluate the corrosion protection of the metal provided by the deposited films.

2. Experimental Procedures

In a closed mold, an alloy of silver and copper with the composition of (wt percent) Ag 85 and Cu 15 was cast. The material was then rolled cold to a thickness of 0.3 mm. The sheet was rolled and cut into 20×20 mm coupons [18]. All coupons were polished to a mirror finish, cleaned with ethanol in an ultrasonic cleaner bath for 10 minutes, then stored for several days in desiccators wrapped in optical paper in accordance with ASTM standards [19]. Without additional purification, commercial O₂ gas (99.9999 percent purity) and HMDSO ([CH₃]₂SiOSi [CH₃]) (Sigma Aldrich) of 98 percent purity were utilized.

2.1. Plasma deposition reactor

Figure (1) depicts a schematic illustration of the RF-plasma assisted CVD employed for the deposition of SiO₂, which comprises a stainless steel chamber measuring 10 cm in diameter and 20 cm long. The chamber is fitted with two 5 cm diameter stainless steel electrodes. The Teflon flanges that separate these electrodes from the chamber wall isolate the electrodes themselves. RF power supply (Coaxial power UK model RFG 1K-13) with (13.56 MHz), 1 kW of power is connected to the chamber via a -type matching network containing two variable air gap capacitors 0-250 pF and an air variable coil. During the experiment, the reflected power was kept at nearly 0W. The reactor was evacuated up to 100 mtorr with rotary pump. Then, HMDSO vapor was pumped into the chamber through a stainless steel bubbler, while oxygen was used as a carrier gas. This chamber had a moderate vacuum, and the total pressure of the discharge cell was changed from 0.2 to 3 Torr. The samples were processed on the grounded electrode at the plasma's floating temperature (T <70 °C). A needle valve and a pressure gauge made it possible to keep the pressure at the desired level by putting RF power into a mixture of hexamethyldisiloxane (HMDSO) and oxygen in the gas phase. Before deposition, Ar-plasma at 100 W and 1 Torr was

used to treat the silver substrates. Table (1) shows the conditions of the experiment.

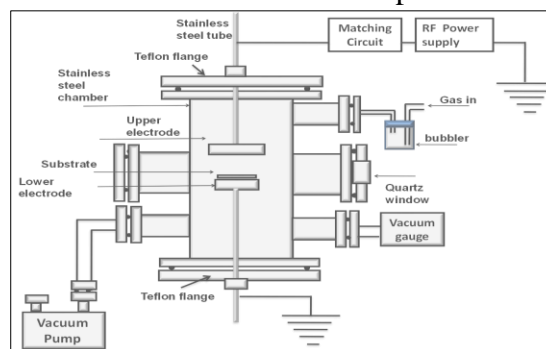


Figure (1) Schematic diagram of the experimental apparatus of the RF-PECVD employed for film deposition.

Table (1) Summary of experimental conditions of PECVD of SiO₂ films

Sample	Power (W)	Time of pre-treatment (min)	deposition time	The used gas for pretreatment at 100 w and 1000 mTorr	
Blank (bare substrate)	---	---	---	---	---
The pre-activated coupon with argon and deposited with argon					
A	200	3	5	Argon	Argon
The pre-activated coupons with argon and deposited with oxygen					
B	100	---	5	Argon	Oxygen
C	200	---	5	Argon	Oxygen
D	250	3	5	Argon	Oxygen
E	300	3	7	Argon	Oxygen

2.2. Characterization techniques

On a JASCO FT-IR-460 plus spectrometer in the reflection mode from 400 and 4000 cm⁻¹, attenuated total reflectance was used to characterize the deposition films (ATR) chemically. Before and after deposition, morphological characterization was done with a scanning electron microscope: Model Zees Sigma 300 VP Field Emission Gun (FEG), stability > 0.2%/h attached to an EDX Unit (Smart EDAX -energy dispersive spectroscopy (EDX)- line ID), with accelerating voltage 0.02 kV - 30 kV, with resolution up to 3072 x 2304 pixel. FESEM. EDX was performed at the Egyptian Petroleum Research Institute, Nasr City, Cairo, Egypt. Morphological, topographical, and roughness measurements were performed on films of silver alloy substrates using Atomic Force Microscope Auto probe cp-research manufactured by Thermo Microscopes operated in contact mode using Silicon Nitride probe model MLCT man-ufactured by Broker. Pros can 1.8 software was used for controlling the scan parameters: (contact mode, scan area

2.5×2.5 μm², scan rate 1 Hz, number of data points 256×256 points) and IP 2.1 software for image analysis. The efficiency of the protective coating SiO_x film was assessed by means of Electrochemical Impedance Spectroscopy (EIS). Electro-chemical impedance measurements were performed in an aerated 0.1M NaCl solution at the laboratory T of 25°C±1, using AUTOLAB 302N, FRA32, Netherlands Impedance. Impedance spectra were recorded at Potential (V) linked with O.C.P. (Open Circuit Potential) value in the frequency range of 5000: 0.02 Hz. The Hydrophobic or hydrophilic characteristics of the deposited film were evaluated by means of contact angle measurement to detect the surface wettability using deionized water as a liquid probe by utilizing a contact angle analyzer model T200 manufactured by Biolin scientific with One Attension Version 2.7 (r5433) software. The colorimetric measurement assisted in determining the resistance of a SiO₂ PECVD deposition to tarnishing visually and quantitatively using Miniscan Ez portable color measurement spectrophotometer: MSEZ-4500S, a measured area of Ø 6 mm and specular component excluded

(SCE), operating with a d/0 SCE measuring geometry. The film thickness was evaluated using a Spectroscopic Ellipsometer PHE-103 Angstrom Ellipsometer as the sample measured at the range of 400-700 nm and the angle of incidence of 70°. After the measurement, data fitting analysis was performed using the fitting algorithms and mathematical modeling to determine the film thickness. The thickness of the deposited layers ranged from 930.12 to 1047.64 nm.

3. Results

FT-IR spectra of the deposited coupons with different parameters, fig. (2) and tab. (2) [20,21]. The most significant absorption bands in the precursor's (HMDSO) standard spectrum, as well as the bond vibrations they correspond to, are 2922-2961 cm⁻¹ (asymmetric stretching in CH₃ groups), 1260 cm⁻¹ (Si-CH₃ wagging (symmetric bending of methyl groups bonded to Si)), 849 cm⁻¹ (rocking of CH₃ in Si-((CH₃)₃)), and 1072 cm⁻¹ (Si-O-Si asymmetric stretching). The structure of the monomer molecule makes it simple to deduce all of these vibrations.

Figure (2) Shows FTIR transmittance spectra of the standard precursor (HMDSO) and the deposited samples A, B, C, D & E.

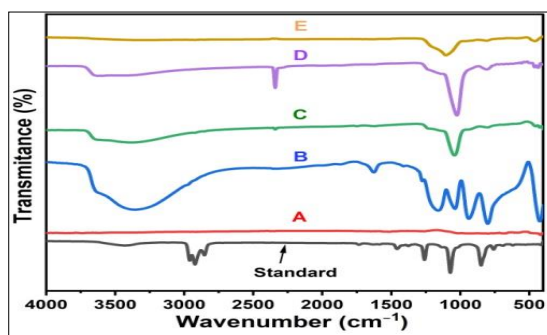


Table (2) FT-IR peak wave numbers and vibrational assignments detected in the experimental samples.

Vibrational assignment	Wave numbers cm ⁻¹ literature [8, 20-21]	Standard precursor (HMDSO)	Sample					
			A	B	C	D	E	
OH stretching in free Si-OH	3300-3400	n.d	n.d	3357	3392	n.d	n.d	
Inorganic Groups								
Silanol groups Si-OH stretching	900-920	n.d	n.d	938	934	n.d	n.d	
Bending mode δ (OH) of surface hydroxyl groups	1635-1735	n.d	n.d	1626	1749	n.d	n.d	
Si-O-Si asymmetric stretching vibration mode	1000-1150	1072	1014	1038-1159	1041	1024	1104	
Si-O-Si bending vibration mode	800	849	796	801	804	807	808	
Si-O-Si Rocking mode	450	450.	419	425	423-453	460	458	
Organic Groups								
C-H asymmetric stretching	2847-2960	2922-2961	2917	2973	2925	n.d	n.d	
Si-CH ₃ wagging (symmetric bending of methyl groups bonded to Si)	1256-1267	1259	1262	1274	1273	n.d	n.d	
Carbonyl group due to C O stretching vibration	1746	n.d	1743	1758	1749	n.d	n.d	
CO ₂ coming from the ambient air	2357	n.d	2348	2355	2341	2342	n.d	

Few features can be observed in the spectra of the deposited coupons with different parameters, as shown in tab. (1) & fig. (2): the Si–O–Si asymmetric stretching absorption bands at 1000–1150 cm^{-1} and other typical Si–O rocking and bending absorption bands at 450 cm^{-1} and 800 cm^{-1} , respectively. With respect of the organic groups, the FTIR absorption spectra of the standard precursor, samples A, B, C, D and E showed the absorption bands of Si–O at 1072 cm^{-1} , 1014 cm^{-1} , 1038–1159 cm^{-1} , 1041 cm^{-1} , 1024 cm^{-1} , 1104 cm^{-1} (stretching) at 849 cm^{-1} , 796 cm^{-1} , 801 cm^{-1} , 804 cm^{-1} , 807 cm^{-1} , and 808 cm^{-1} (bending), respectively, and at 450 cm^{-1} , 419 cm^{-1} , 425 cm^{-1} , 423–453 cm^{-1} , 460 cm^{-1} , and 458 cm^{-1} (Si–O–Si rocking mode) respectively. OH stretching in free Si–OH was detected only for samples B and C at 3329 cm^{-1} and 3392 cm^{-1} . Also, the features of silanol groups (Si–OH) were detected for samples B and C at 938 cm^{-1} and 934 cm^{-1} (bending), respectively. The bending mode and (OH) of surface hydroxyl groups was only for samples B and C at 1626 cm^{-1} and 1749 cm^{-1} . With respect to the inorganic groups detected in the standard precursor, samples A, B, and C showed the absorption bands of 2922–2961 cm^{-1} , 2917 cm^{-1} , 2973 cm^{-1} , and 2925 cm^{-1} , respectively. Si–CH₃ wagging or symmetric bending of methyl groups bonded to Si was detected for the standard precursor, samples A, B, and C at 1259 cm^{-1} , 1262 cm^{-1} , 1274 cm^{-1} , and 1273 cm^{-1} , respectively. The carbonyl group due to C–O stretching vibration was detected only for samples (A, B, and C) at 1743 cm^{-1} , 1758 cm^{-1} , and 1749 cm^{-1} . This group was not detected for sample E. CO₂ from the ambient air was detected for samples A, B, C, and D at 2348 cm^{-1} , 2355 cm^{-1} , 2341 cm^{-1} , and 2342 cm^{-1} , respectively. Organic groups weren't detected for samples D and E as the low carbon content and consequently SiO₂-like character of the deposited films of samples D and E was confirmed by the low intensity of the CH_x symmetric and

asymmetric stretching bands at 2900–2960 cm^{-1} and the absence of the other typical CH_x bands, such as the Si–CH₃ rocking vibration at 840 cm^{-1} and the CH₃ symmetric bending in Si–CH₃ at 1260 cm^{-1} . Surface Si–OH groups situated and silanol groups Si–OH stretching absorption bands weren't detected for samples (A, D, and E). CO₂ from the ambient air was not detected for sample E due to the high power and the long time of the deposition. The results of SEM and EDX analyses showed the surface morphology and analysis of the samples. Figure (3-a) shows the surface of the silver-copper alloy substrate of sample (A) after pre-activation and deposition with argon plasma. Figure (3-b) represents the substrate after aging with the tarnishing test, whereas Figure (4-a & b) represent sample (B). Figure (5-a) reveals the deposited film on the sample after activation with argon plasma and deposition with oxygen plasma for five minutes, while Figure (5-b) reveals the same sample after aging with the tarnishing test. Figure (5-a & b) represent sample (E). Figure (5-a) reveals the deposited film on the sample after activation with argon plasma and deposition with oxygen plasma for seven minutes, while Figure (5-b) reveals the same sample after aging with the tarnishing test.

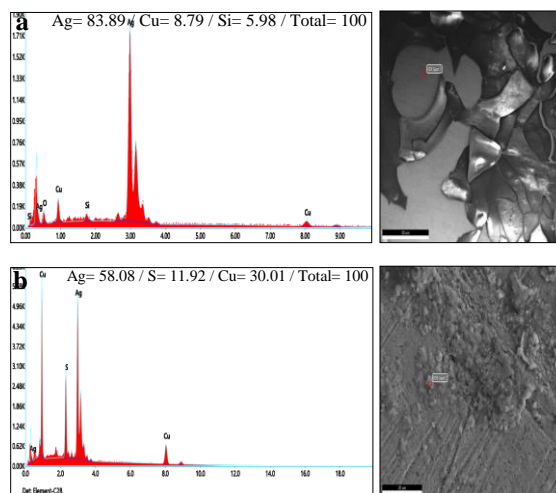


Figure (3) Shows **a.** surface of the silver-copper alloy substrate after pretreatment with argon plasma, **b.** the substrate after aging with tarnishing test.

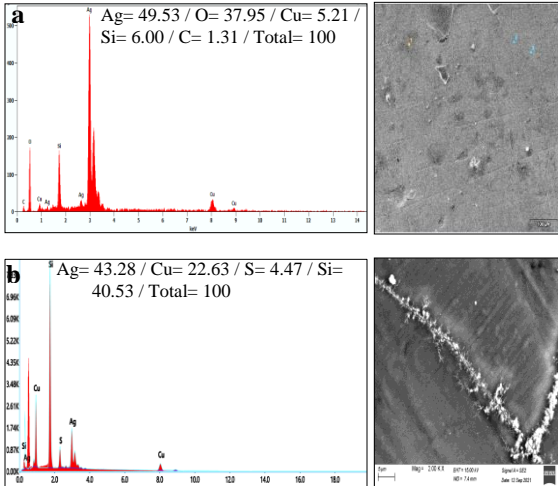


Figure (4) Shows **a.** the deposited film on the sample after activation with argon plasma and deposition with oxygen plasma for 5 minutes, **b.** the same sample after aging with tarnishing test.

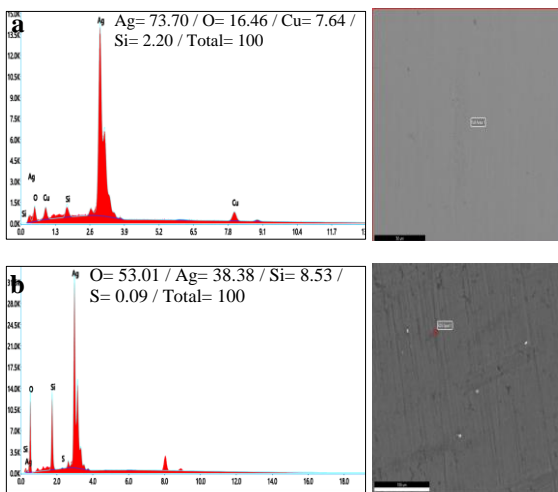


Figure (5) Shows **a.** the deposited film on the sample after activation with argon plasma and deposition with oxygen plasma for 7 minute, **b.** the same sample after aging with tarnishing test.

Sample (A), which was a pre-activated and deposited sample with only argon plasma, showed poor adhesion and homogeneity between the deposited thin film and the irregular silver alloy substrate, fig. (3). The cracks and pinholes in coatings could form direct paths between the corrosive environment and the substrate. Sample (B), which was pre-activated with argon plasma and then deposited with O₂/HMDSO mixtures

at power 100, covered the irregular defects of the substrate surface but showed the presence of carbon after deposition, fig. (4-a) and cracks through the deposited film after aging, fig. (4-b). Additionally, the formation of sulfide corrosion products caused the blistering of the film and its detachment from the metal substrate. Sample (E), the substrate that was pre-activated with argon plasma and then deposited with O₂/HMDSO mixtures for seven minutes at 300 W, covered the rough spots on the substrate surface, fig. (5-a). This thin film was deposited uniformly on the surface and had a high degree of adhesion and adaptability to the surface morphology, even after aging, fig. (5-b). When dealing with corrosion protection, the characterization of surface energy is an important issue; measuring the water contact angle test is required. Water contact angle measurements demonstrated that the values of the contact angle of the bulk coupon were 77.19°, while after deposition, it ranged from 94.61° for the sample (A), 85.68° for sample (B), 87.43° for sample (C), 104.34° for sample (D), to 106.68° for sample (E), as shown in tab. (3) & fig. (6).

Table (3) The contact angle of the deposited the blank and samples A, B, C, D and E

Sample	Right angle	Left angle	Average of the angle
Blank	79.99	74.39	77.19
A	98.68	90.54	94.61
B	89.39	81.97	85.68
C	88.42	87.43	87.43
D	104.70	103.99	104.34
E	108.90	104.46	106.68

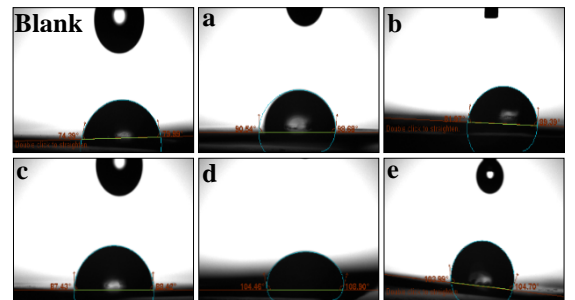


Figure (6) Shows contact angles for the blank sample and the deposited samples A, B, C, D & E

AFM 2 dimensional and 3 dimensional micrographs of the blank sample revealed the

inhomogeneous surface with an average roughness (Ra) of 30.39 nm, fig. (7-a & b). For sample (A), the image revealed the smooth surface of the deposited layer with (Ra values 11.55 nm), fig. (7-c & d) and the presence of small sizes of particles with the size of the particles that ranged from 148.8 nm to 184.4 nm, fig. (8). Sample (B) was pre-activated with argon and deposited with oxygen under power 100. The roughness of the deposited sample was higher than sample (A) with (Ra values of 17.33 nm), fig. (7-e & f). The coating surface morphology was fairly regular, with only a few high big bumps. The size of the particles ranged from 84.3 nm to 118.5 nm, fig. (8). Sample (C) was pre-activated with argon and deposited with oxygen under power 200. The roughness of the deposited sample increased with (Ra values of 25.45nm), fig. (9-a & b). The size of the particles ranged

from 83.51 nm to 96.12 nm, fig. (10). Sample (D) was pre-activated with argon and deposited with oxygen under power 250. The roughness of the deposited sample increased with (Ra values of 42.26 nm), fig. (9-c & d). Fine particles nucleated and grew into progressively small particle aggregates with a deposition time of 5 minutes, the deposited layer was homogenous more than others, and the coating thickness was 955.27 nm. The size of the particles ranged from 172.7 nm to 241.2 nm, fig. (11). Sample (E) was pre-activated with argon and deposited with oxygen under power 300. The roughness of the deposited sample increased with (Ra values of 47.73 nm), fig. (9-e & f). The size of the particles ranged from 84.88nm to 106.1 nm, fig. (12). Also, the deposition time was seven minutes, and the coating thickness was 1047.64 nm.

Table (4). Physical characteristics of samples.

Sample	ΔE	Rough (Rms) (nm)	Ave Rough (Ra) (nm)	Contact angle, θ (deg)	Coating thickness (nm)	Protective efficiency %
Blank (bare substrate)	----	35.79	30,39	77.19	----	-----
<i>The pre-activated coupon with argon and deposited with argon</i>						
A	8.59	14.53	11.55	94.61	939.53	50.92
<i>The pre-activated coupons with argon and deposited with oxygen</i>						
B	5.11	23.80	17.33	85.68	930.12	82.80
C	3.87	33.73	25.45	87.43	----	86.54
D	3.22	51.22	42.26	104.34	955.27	88.97
E	2.42	61.22	47.73	106.68	1047.64	95.60

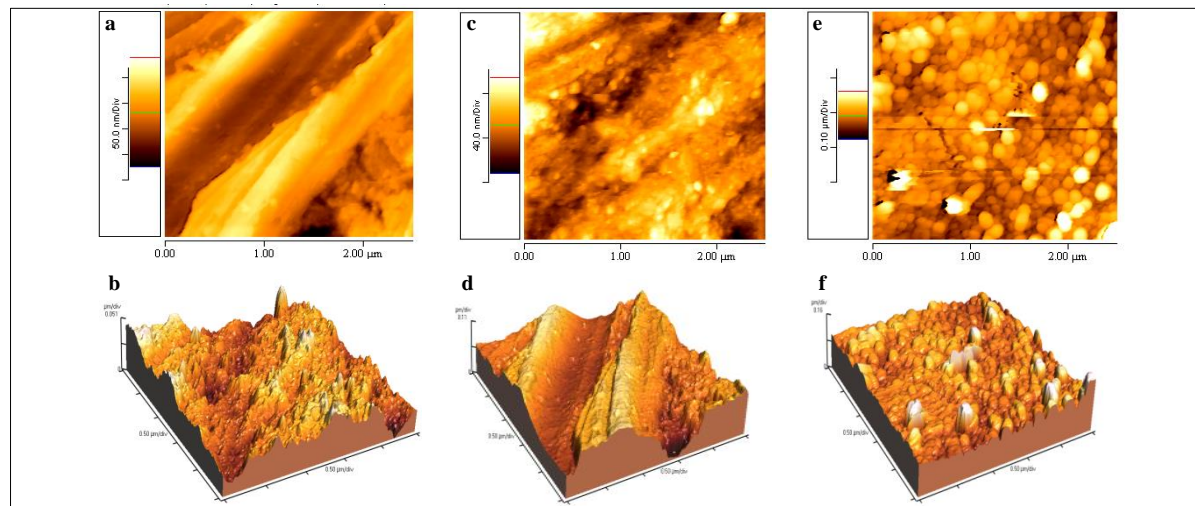


Figure (7) Shows **a.** & **b.** revealed the inhomogeneous surface of the blank sample, **c.** & **d.** 2d and 3d of the pre-activated sample with argon and deposited with argon plasma, power 200, **e.** & **f.** 2d and 3d of the pre-activated sample with argon and deposited with oxygen plasma, power 100

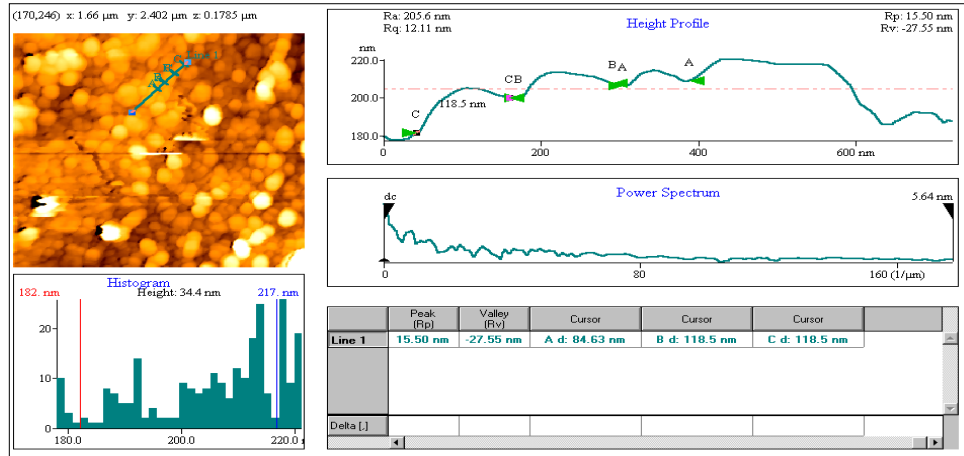


Figure (8) Shows the presence of particles of sample B

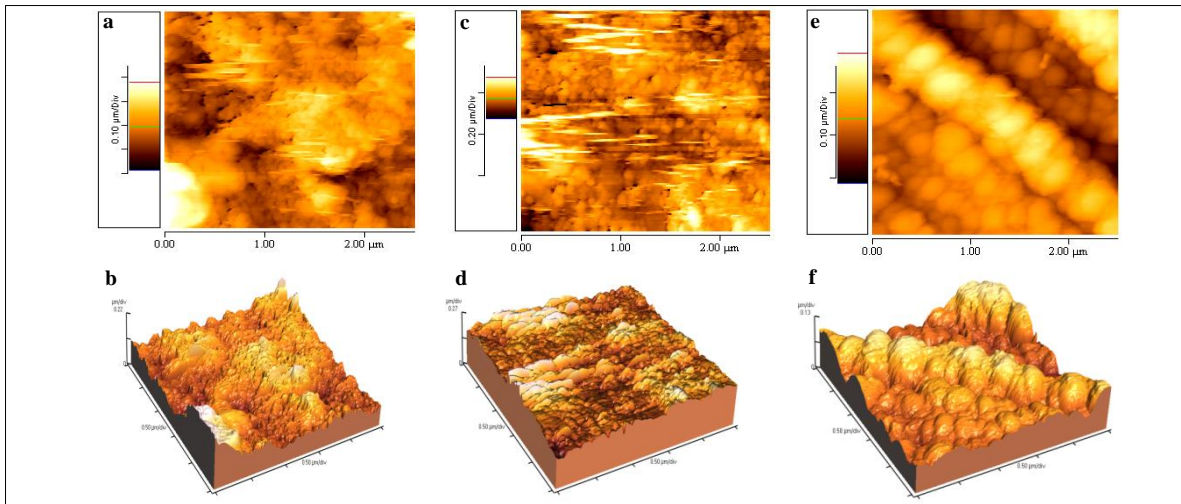


Figure (9) Shows **a.** & **b.** 2d and 3d of the pre-activated sample with argon and deposited with oxygen plasma, power 200, **c.** & **d.** 2d and 3d of the pre-activated sample with argon and deposited with oxygen plasma, power 300, **e.** & **f.** 2d and 3d of the pre-activated sample with argon and deposited with oxygen plasma, power 250

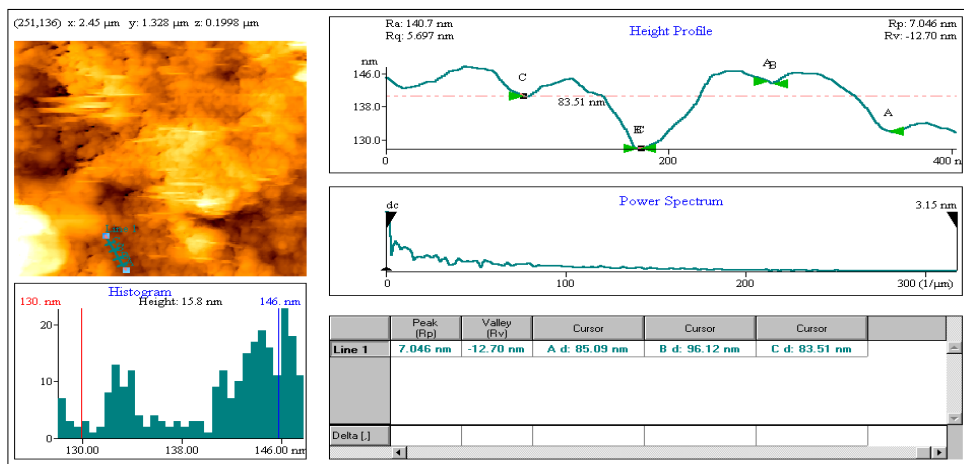


Figure (10) Shows the presence of the size particles of sample C

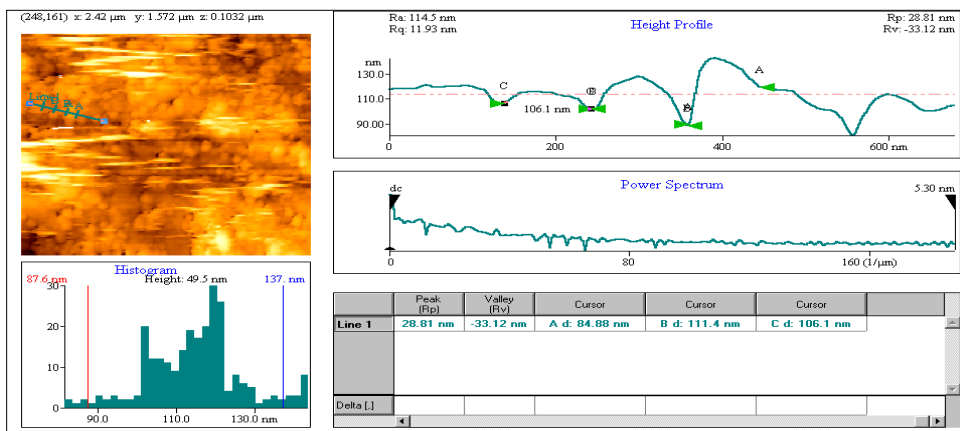


Figure (11) Shows the presence of the size particles of sample D.

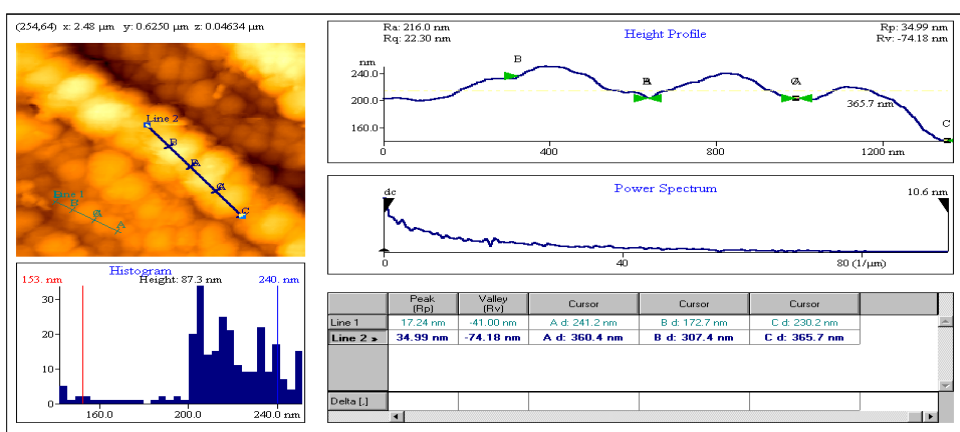


Figure (12) Shows the presence of the size of large particles of sample E

The optical observation and quantitative colorimetric measurements revealed that the SiO₂ layer was significantly more resistant to tarnishing after PECVD deposition. The tarnishing susceptibility of the blank and coated samples was determined by estimating the average of (ΔE) after accelerated aging. The tarnishing test was carried out by exposing the samples to a saturated sulfide atmosphere, followed by a simple corrosion test at 90% relative humidity. For 24 hours, the samples were placed in a desiccator with 0.5g/l sodium sulfide solution and a saturated potassium sulfate solution to raise the relative humidity to 97.3% [22]. Color change measurements (ΔE) for the blank sample and the different parameters of the deposited samples, tab. (5). The corrosion protection of the thin film coating on the metal subst-

rate in 0.1M NaCl solution was investigated using electrochemical impedance spectroscopy (EIS). All the coating films presented nearly similar Nyquist plot shapes compared to the bare metal, fig. (13). To explain the influence of the different plasma parameters on the protective properties of SiO_x thin films, the experimental data were fitted by considering a simple equivalent circuit, as shown in fig. (14). The parameter used to estimate the protection efficiency τ (%) for different films was calculated as the following equation. $\tau = 100 * (R_t - R_{t,0}) / R_t$. The efficiency of sample A, which was pre activated and deposited with argon plasma at 200 W, presented the least protective coating efficiency of 50.92%. In comparison, sample (B), which was pre-activated with argon plasma and deposited with the mixture of oxygen and HMDSO at 100W, showed a

slightly better performance of 82.80%. Sample (C), which was pre-activated with argon plasma and deposited with the mixture of oxygen and HMDSO at 200 W, showed enhanced results of 86.54%. Sample (D) was pre-activated with argon plasma and deposited with the mixture of oxygen and HMDSO at 250 W and showed enhanced results of 88.97%. Sample (E), which was pre-activated with argon plasma and deposited with the mixture of oxygen and HMDSO at 300 W, gave the best protective efficiency of 95.60%.

Table (5) ΔE of the reference samples and samples after aging

Samples after aging	I	a	b	ΔE
A	50.51	-6.15	-2.01	8.59
	54.75	-12.98	-9.14	
B	105.8	68.27	12.06	5.11
	109.4	52.2	13.51	
C	53.37	-8.22	-13.40	3.87
	55.77	-12.03	-15.30	
D	88.65	35.31	17.80	3.22
	88.67	27.82	16.30	
E	58.93	-21.64	-8.44	2.42
	60.17	-23.71	-11.74	

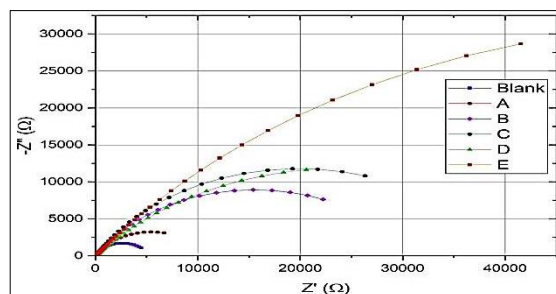


Figure (13) Shows Nyquist plots of EIS measured in 0.1M NaCl of plasma coated films compared to the bare metal

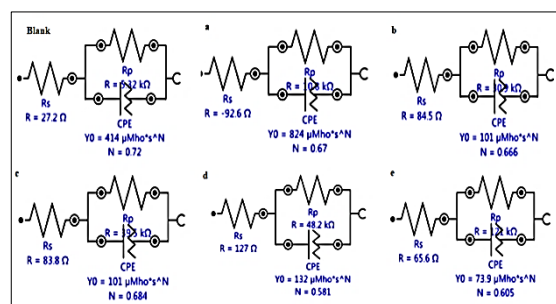


Figure (14) Shows the equivalent model of system for the blank and the deposited samples

4. Discussion

It was demonstrated for sample (A) that, despite the argon ion's larger atomic mass

than oxygen, the action of the gas was negligible since the partial pressure was too low when it was employed to activate the surface and transport the monomer (HMDSO). The deposited film did not contain any OH groups. Samples (B & C) revealed the role of the low power by the presence of the OH groups, while sample (D) revealed the effect of increasing the power to 250 by the disappearance of the OH groups. However, there was a peak representing the CO₂ coming from the ambient air. In sample (E), by increasing the power to 300 and the time of the deposition process to 7 min, it was found that the deposited thin film only contained the vibrational assignment of SiO₂, and the FTIR spectra did not contain any organic compounds or any OH groups. Higher ion bombardment energy and dose, which are expected to improve OH group abstraction as well as the removal of residual organic groups, can be attributed to the decrease in Si-OH groups with increasing input power. The low concentration of silanols is an important factor in the use of these coatings as protective layers because silanols result in a less packed molecular structure in the coatings, resulting in a higher permeability to water and reactants. Because silanol groups are frequently reactive on their own, they can contribute to the instability of the coating [23]. Therefore, we can say that the growth rate of the film and the carbon content in the film are measured as a function of the O₂ and HMDSO admixture. SiO_x inclusions and the degree of "inorganic", which are both related to the Si content of the coatings, as well as the thickness of the layer, are additional factors that can affect the intensity of Si-related absorptions [24, 25]. The FTIR analysis results show that increasing input power has a major impact on coating chemical composition by removing organic groups from the thin film that is being deposited [21]. To prevent additional oxidation of surfaces, particularly metals,

short exposures to inert gases like argon plasma may be chosen for cleaning. By ion bombardment and physical ablation, argon plasma removes contaminations from surfaces without reacting to them. Also, the addition of oxygen into the gas mixture increases HMDSO depletion and the growth rate and results in the deposition of carbon-free films. The surface reaction is responsible for the carbon removal from the growing film [26,27]. The results of SEM-EDX analysis revealed the role of the pre-activation with argon plasma in removing the residues of contaminants retained loosely and stimulating the surface to boost bonding strength [28]. Additionally, brief exposure to active plasmas, such as oxygen plasma, caused the substrate to develop reactive sites that could then be used to plasma polymerize the precursor molecule to enable covalent bonding between the substrate and the film being deposited [29], especially by increasing the input power and the time of the deposition. By increasing the time of the deposition, the thickness of the deposited thin film increased. Water contact angle measurements demonstrated that sample (A), which was pre-activated and deposited with argon at 200 W, did not produce silanol groups, and its contact angle was 94.61° . The contact angle of samples (B) and (C), which were pre-activated with argon and deposited with oxygen plasma at 100 W and 200 W, respectively, were 85.68° and 87.43° . The contact angle of samples (B and C) was low due to the presence of silanol groups. By increasing the input power for samples (D and E) at 250 and 300, respectively, the contact angle ranged from 104.34° to 106.68° . So, the composition and the morphological structure of the deposited films change with the deposition conditions and determine the gas barrier performances [30]. For sample (A), it was observed that the pre-activation and deposition with argon plasma at 200W revealed that the presence of argon modifies

the plasma composition and the deposition rate could create some defects and low roughness. The presence of argon alters the plasma composition and deposition rate and causes some defects [31]. Argon plasma was only used for the pre-activation of the surface, and oxygen plasma was then utilized for the deposition process at different power. As for samples (B and C), roughness increased gradually due to the bombardment of additional species in the plasma. This result illustrated that by increasing the power, the roughness of the deposited thin film increased, as shown in table (4). It also pointed to the role of high power 300 W in increasing the roughness of the coated sample to (rms values of 47.73 nm) and increasing the grain size and the importance of increasing the time of the deposition process to (7 min), which helped in increasing the thickness of the deposited layer. Fine particles nucleated and grew into progressively larger particle aggregates. Also, increasing the deposition time to seven minutes was adequate to increase the coating thickness to 1047.64 nm, this formed particles which were deposited and stacked on the metallic surface. AFM images showed that the grain size and surface RMS roughness were influenced by the film thickness. Increasing thickness indicated that the crystalline quality of the films was improved. The grain size and the RMS roughness increased with increasing thickness [32]. It showed that the type of plasma, exposure time, and exposure power all have a significant impact on surface chemistry and morphology [33]. As the deposition time was increased, the agglomerates grew in size and became dominant, forming a micro-nano structured surface with a high surface roughness required for extreme water repellency or super hydrophobicity [18]. The result of color change measurement of the coated samples revealed that sample (E) gave the best result as it displayed the least average of ΔE 2.42. Whereas, sample (B,

C and D) displayed the average of ΔE 3.22, 3.87 and 5.11 respectively. These results emphasize the role of pretreatment with argon and deposition with oxygen plasma, the high power for the deposited film to protect the silver-copper alloys as well as the importance of increasing the time. But the pretreatment and deposition with argon plasma was not efficient as it displayed the highest average of ΔE 8.59. A significant increase in the size of the impedance diagram indicates a significant improvement in the metal surface's corrosion resistance. This finding demonstrates that the coating and substrate are interfacially bonded. The findings also showed that the oxygen plasma treatment improves the adhesion of the substrate to the coating layer.

5. Conclusion

Argon plasma was more efficient in the pre-activation of the surface before deposition than oxygen plasma with low surface roughness. Argon plasma treatment had little effect on the aromatic rings, surface region, and the formation of new species, most likely ethers and esters. But for the deposition process, oxygen plasma was more effective in promoting adhesion properties than argon, an inert gas. The deposition of carbon-free SiO_2 films from HMDSO is thought to be possible only if an additional oxidizer, such as O_2 or N_2O is added to the source gas. The protection effect was higher for coatings deposited in oxygen-rich plasmas at high input power and increasing the time of the deposition process. Because under these experimental conditions, coatings were made with fewer flaws and no silanol groups. The thickness of the deposited film was also made thicker.

References

- [1] Angelini, E. & Grassini, S. (2013). Plasma treatments for the cleaning and protection of metallic heritage artefacts, in: Dillmann, P., Watkinson, D., Angelini, E., et al. (eds.) *Corrosion & Conservation of Cultural heritage Metallic Artefacts*, Woodhead Pub. Limited, Cambridge, pp. 552-569.
- [2] Reti, A. & Mridha, S. (2001). Silver: Alloying, properties, and applications, in: Buschow, K., Cahn, R. & Veysière, P. (eds.) *Encyclopedia of Materials: Science and Technology* 2nd ed., pp. 8618-8621
- [3] Luxford, N. & Thickett, D. (2007). Preventing silver tarnish—lifetime determination of cellulose nitrate lacquer, in: Degriigny, C., Robert, V., ICOM, et al (eds.) *Metal 07, Interim Meeting of the ICOM-CC Metal Working Group*, Rijksmuseum, Amsterdam pp. 88-93.
- [4] Tsai, P., Chen, P. & Lee, Y. (2018). Development and characterization of anticorrosion and antifriction properties for high performance polyurethane/graphene composite coatings, *Coatings*, Vol. 8 (250), doi: 10.3390/coatings8070250.
- [5] Yuan, X., Yue, Z., Liu, Z., et al., (2016). Effect of siloxane-modified polyacrylate on water uptake and anticorrosion mechanism of silicone-epoxy coatings, *J. of Coatings Technology and Research*, Vol. 13 (1), pp. 123-132.
- [6] Lasorsa, C., Perillo, P. & Morando, P. (2010). Protective $\text{Si}_x\text{O}_y\text{C}_z$ coatings on steel prepared by plasma activated chemical vapour deposition, *Surface & Coatings Technology*, Vol. 204 (16), pp. 2813-2816.
- [7] Lee, Y-S. & Lee, S-H., Kwon, J-D., et al. (2017). Silicon oxide film deposited at room temperatures using high-working pressure plasma-enhanced chemical vapor deposition: Effect of O_2 flow rate, *Ceramics Int.*, Vol. 43 (1)4, pp. 10628-10631.
- [8] Benítez, F., Martínez, E. & Esteve, J. (2000). Improvement of hardness in plasma polymerized hexamethyldisiloxane coatings by silica-like surface modification, *Thin Solid Films*, Vol. 377-378, pp. 109-114.
- [9] Trunec, D., Zajickova, L., Buršíková, V., et al. (2007). Deposition of hard thin films from HMDSO in atmospheric pressure dielectric barrier discharge, *J. of Physics D: Applied Physics*, Vol. 43, (22), doi: 10.1088/0022-3727/43/22/225403.

- [10] Zanini, S., Riccardi, C., Orlandi, M., et al. (2005). Surface properties of HMDSO plasma treated polyethylene terephthalate, *Surface and Coatings Technology*, Vol. 200 (1-4), pp.953-957.
- [11] Saloum, S., Alkhaled, B., Alsadat, W., et al. (2018). Plasma polymerized hexamethyldisiloxane thin films for corrosion protection, *Modern Physics Letters B*, Vol. 32 (03), doi: 10.1142/S0217984918500367.
- [12] Saloum, S., Abou Shaker, S., Alkafri, M., et al. (2019). Effect of surface modification on the properties of plasma-polymerized hexamethyldisiloxane thin films, *Surface Interface Analysis*, Vol. 51, pp. 754-762.
- [13] Choudhury, A., Barve S., Chutia, J., et al. (2011). RF-PACVD of water repellent and protective HMDSO coatings on bell metal surfaces: correlation between discharge parameters and film properties, *Applied Surface Science*, Vol. 257 (20), pp. 8469-8477.
- [14] D'Agostino, R. Fracassi, F. Palumbo, F., et al. (2005). Protection of silver-based alloys from tarnishing by means of plasma-enhanced chemical vapor deposition, *Plasma Process Polymer*, Vol. 2 (2), pp. 91-96.
- [15] Trinh, H., Nguyen, D., Hossain, M., et al. (2019). Deposition of superhydrophobic coatings on glass substrates from hexamethyldisiloxane using a kHz powered plasma jet, *Surface and Coatings Technology*, Vol. 361, pp. 377-385.
- [16] Yan, X., Liu, G., Yang, J., et al. (2019). In situ surface modification of paper-based relic with atmospheric pressure plasma treatment for preservation purposes, *Polymers*, Vol. 11(5), doi: 10.3390/polym11050786.
- [17] Blanchard, N., Naik, V., Geue T., et al. (2015). Response of plasma-polymerized hexamethyldisiloxane films to aqueous environments, *Am. Chemical Society*, Vol. 31 (47), pp. 12944-12953.
- [18] Angelini, E., Grassini, S., Ingo, G., et al. (2010). Surface analysis of SiO₂-like high-barrier thin films for protection of silver artefacts, *Surface and Interface Analysis*, Vol. 42 (6-7), pp. 666-670.
- [19] ASTM Int. (2003). *Annual book of ASTM standards, Section 3: Metals test methods and analytical procedures*, G 1-90: *Standard practice for preparing, cleaning and evaluating corrosion test specimens*, ASTM, USA.
- [20] Zanini, S., Riccardi, C., Orlandi, M., et al. (2007). Characterisation of SiO_xCyHz thin films deposited by low-temperature PECVD, *Vacuum*, Vol. 82 (2), pp. 290-293.
- [21] Angelini, E., D'Agostino, R. Fracassi, F., et al. (2002). Surface analysis of PECVD organosilicon films for corrosion protection of steel substrates, *Surface and Interface Analysis*, Vol. 34 (1), pp. 155-159.
- [22] McEwan, J., Scott, M. & Goodwin, F. (2005). The development of an accelerated tarnish test for sterling silver. in: Yuan, Z. & Xue hui, Z. (eds.) *16th Int. Corrosion Cong.*, Int. Corrosion Council, Chinese Society for Corrosion and Protection, Beijing pp. 1-9.
- [23] Awang, M., Khalili, A. & Pedapati, S. (2020). A review: Thin protective coating for wear protection in high-temperature application. *Metals*, Vol. 10 (1), doi: 10.3390/met10010042.
- [24] Krueger, T., Hansen, L. & Kersten, H. (2020). Deposition of SiO_x thin films using hexamethyldisiloxane in atmospheric pressure plasma enhanced chemical vapor deposition, *IOP J. of Physics: Conf. Series*, Vol. 1492 (1), doi: 10.1088/1742-6596/1492/1/012023.
- [25] Mozetič, M. (2020). Plasma-stimulated super-hydrophilic surface finish of polymers, *Polymers*, Vol. 12(11), doi:10.3390/polym12112498
- [26] Patelli, A., Verga, E., Nodariet, L., et al. (2018). A customised atmospheric pressure plasma jet for conservation

- requirements, *IOP Conf. Ser.: Mater. Sci. Eng.*, doi:10.1088/1757-899X/364/1/012079.
- [27] Reuter, R., Hoyer, K., Ellerweg, D., et al. (2011). The role of oxygen and surface reactions in the deposition of silicon oxide like films from HMDSO at atmospheric pressure, *Plasma Processes and Polymers*, Vol. 9.(11-12), doi: 10.1002/ppap.201100146
- [28] Tiño, R., Viárová, K., Krčma, F., et al. (2021). Plasma technologies in preservation of cultural heritage, Ch. 3, in: Tiño, R., Viárová, K., Krčma, F., et (eds.) *Plasma Technology in the Preservation and Cleaning of Cultural Heritage Objects*, 1st ed., CRC Press, pp. 11-42
- [29] Chifen, A., Jenkins, A., Knoll's, W., et al. (2007). Adhesion improvement of plasma-polymerized maleic anhydride films on gold using HMDSO/O₂ adhesion layers, *Plasma Processes and Polymers*, Vol. 4(9), pp. 815-822.
- [30] Batey, J. & Tierney, E. (1986). Low-temperature deposition of high-quality silicon dioxide by plasma-enhanced chemical vapor deposition, *J. of Applied Physics*, Vol. 60 (9), pp. 3163-3145,
- [31] Keil, M., Rastomjee, C., Rajagopal, A., et al. (1998). Argon plasma-induced modifications at the surface of polycarbonate thin films, *Applied Surface Science*, Vol. 125 (3-4), pp. 273-286.
- [32] Xin, Z., Xiao-Hui, S. & Dian-Lin, Z. (2010). Thickness dependence of grain size and surface roughness for dc magnetron sputtered Au, *Chinese Physics B*, Vol. 19 (8), doi: 10.1088/1674-1056/19/8/086802
- [33] Slepíčka, P., Trostová, S., Kasálková, N., et al. (2012). Surface modification of biopolymers by Argon plasma and thermal Treatment, *Plasma Processes & Polymers*, Vol. 9. (2), pp. 197-206.